scientific reports

Check for updates

OPEN

Facile preparation and adsorption performance of low-cost MOF@cotton fibre composite for uranium removal

Aili Yang✉, Zhijun Wang & Yukuan Zhu

A novel composite MOF@cotton fibre (HCF) was prepared and characterized by FTIR, SEM, XPS and TGA. The effect of various parameters on the adsorption efficiency, such as the solution pH, contact time, initial U(VI) concentration and temperature, was studied. The maximal sorption capacity (Q_m) is 241.28 mg g^{-1} at pH 3.0 for U(VI) according to the Langmuir isotherm adsorption model, and the kinetic and thermodynamic data reveal a relatively fast entropy-driven process (ΔH^0 = 13.47 kJ mol^{-1} and ΔS^0 = 75.47 J K^{-1} mol^{-1}). The removal efficiency of U(VI) by HCF is comparable with that of pure cotton fibre and as-prepared MOF (noted as HST). However, the HST composite with cotton fibre significantly improved the treatment process of U(VI) from aqueous solutions in view of higher removal efficiency, lower cost and faster solid–liquid separation. Recycling experiments showed that HCF can be used up to five times with less than 10% efficiency loss.

Uranium (U) is a key radioactive element for nuclear fuel in the nuclear reactors. The remarkable development of nuclear activities related to U such as mining, refinement and recovery of U is of critical importance for the continued development of nuclear energy[1,2]. To decrease the release of U into the environment and contamination risks in case of incidents or nuclear events, an adsorption approach based on various high-efficiency sorbents has been proposed and attracted considerable attentions[3–7]. Adsorption has been examined as an alternative method to remove U from aqueous solutions due to its simple operation, low cost, energy saving, high efficiency, etc Cellulose and their derivatives have achieved extensive attention due to their advantages such as the most abundant resource, biocompatibility, inexpensiveness and eco-friendliness[8,9]. However, pure cellulose generally exhibits poor capacity in practical applications and must be chemically modified[10–12]. The composite of cellulose with other substances is an efficient approach to enhance their performance and extend their applications[13–16].

As a class of important porous materials, metal–organic frameworks (MOFs) have outstanding characteristics including extra-high surface areas, diverse functionalities, linkers tailorability, acid and base robustness and tunable aperture[17,18]. Thus, they have great potentials in diverse domains such as gas storage and separation[19], sensing[20], adsorption[21–23], biomedicine[24], magnetism[25], luminescence[26], environmental remediation[27–29], and catalysis[30,31]. MOFs@cellulose composites have been proven to provide better benefits for their versatile applications than pure cellulose or MOFs[32]. However, most of the recent achievements have highlighted the antibacterial properties[33–37], gas adsorption[38] and pollutant removal[39–42] of MOF@cellulose composites. To our best knowledge, the integration of HKUST-1 with cellulose to synergistically enhance their intrinsic prominent properties for the removal of U(VI) has never been reported, except for a few reports on the removal of U(VI) using cellulose derivatives[43–52]. In addition, the production cost of cellulose derivatives must be significantly reduced to further improve their real applications. Our research has the following contributions: (i) a novel, facile and low-cost method to prepare MOF@cotton fibre (HCF) composite, which uses a much cheaper benzoic acid (BA; the cost of the analytical-grade product is 16.4 ¥/250 g) as the ligand to replace part of the traditional ligand trimesic acid (H_3BTC to synthesize HKUST-1; the cost of the analytical-grade product is 566 ¥/500 g); (ii) fibriform HCF, which is very easily separated from the liquid phase; (iii) favourable adsorption efficiency for U(VI), where the maximal adsorption capacity is 241.28 mg g^{-1}.

In the present study, a novel MOF@cotton fibre (HCF) composite was facilely synthesized by a simple hydrothermal method. To characterize the obtained materials, X-ray photoelectron spectroscopy (XPS), FT-IR

Institute of Materials, China Academy of Engineering Physics, Jiangyou Sichuan 621907, China. ✉email: yang770117@sina.com

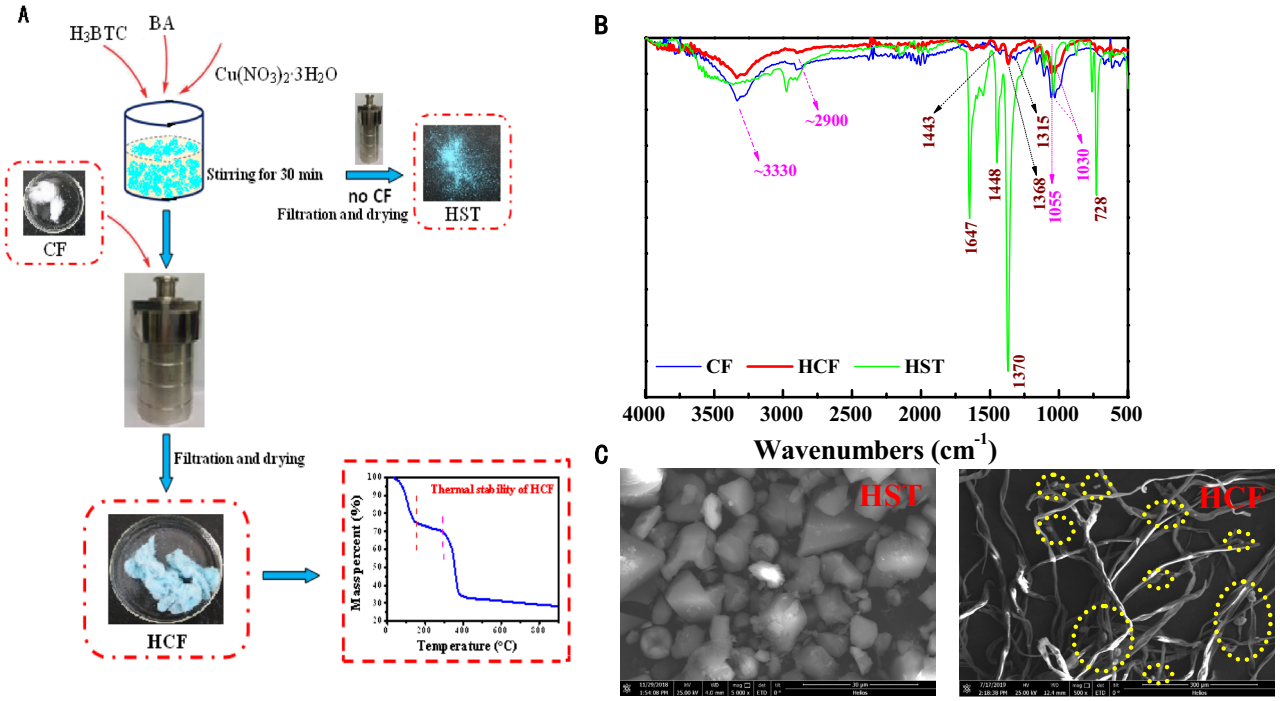

Figure 1. (**A**) Preparation flow diagram and thermal stability of HCF and morphology characterization; (**B**) FTIR spectra of the samples; (**C**) SEM images of HST (×5000) and HCF (×500).

spectroscopy (FTIR), scanning electron microscopy (SEM) and thermogravimetric analysis (TGA) were used. The effects of a few critical parameters (pH value, contact time, initial U(VI) concentration and temperature) and the adsorption kinetics, adsorption isotherms and reusability of HCF were investigated in detail.

Results and discussion

Characterization. The preparation flow diagram and FTIR and SEM image characterization of the samples are shown in Fig. 1. To reduce the preparation cost of the adsorbent, BA with lower cost was used as the ligand to replace part of the traditional ligand H_3BTC. The blue powder product HST was obtained by a simple solvothermal method. While we added CF into the HST precursor (Cu^{II}, BA and H_3BTC) solution for the solvothermal synthesis, the blue fibrous product HCF was fabricated (see Fig. 1A). The thermal stability of HCF was shown in Fig. 1A.

The functional group structures of the samples were characterized by FTIR spectra as shown in Fig. 1B. The characteristic peaks at 1370 cm^{-1}, 1448 cm^{-1} and 1647 cm^{-1} were attributed to C–O, C=O and aromatic C=C of H_3BTC, respectively[53]. The characteristic peaks at 1368 cm^{-1} and 1443 cm^{-1} appeared in the FTIR of HCF. Similar characteristic peaks at ~3330 cm^{-1}, ~2900 cm^{-1}, 1055 cm^{-1} and 1030 cm^{-1} appeared in the IR of both HCF and CF. These results show that HST combined with CF successfully to produce HCF.

The surface morphologies of HST and HCF observed in SEM images are shown in Fig. 1C. The as-synthesized HST particles with octahedral and spherical shape (highlighted as yellow dashed circles) were distinctly observed in the surfaces of CF. XPS was used to study the composition and valence of HCF and CF. Figure 2 shows the XPS survey spectra of HCF and CF. In Fig. 2 and the insert, two main peaks at 930.2 and 952.0 eV, which are ascribed to Cu $2p_{3/2}$ and Cu $2p_{1/2}$ signals, correspond to the characteristic peak of Cu^{2+} in the XPS survey spectrum of HCF, which indicates the presence of HST in the composite HCF[54].

Effect of the pH and ion strength on the U removal. The chemistry species of uranium in the solutions significantly varies at different pH, which makes the solution pH greatly affect the adsorption efficiency. The effect of the solution pH of 2–8 and ion strength with different concentrations of $NaClO_4$ (0.001, 0.01, 0.1 and 1.0 M) on the uranium adsorption is shown in Fig. 3. In Fig. 3 (insert), the removal rate of U(VI) by HCF and CF was maximal at pH = 3. It is well known that the most predominant uranium species is UO_2^{2+} at low pH; therefore, the removal rate was low due to the competition between abundant H^+ and UO_2^{2+} ions[55]. With increasing solution pH when U is mainly present as negatively charged species $(UO_2)_3(OH)_7^-$ and $(UO_2)(OH)_3^-$, the removal efficiency increased due to the electrostatic attraction between the negatively charged U(VI) species and the positively charged sorbent[56]. When the pH further increased, the hydrolysation of UO_2^{2+} and formation of U(VI)-carbonate species $(UO_2)_2(CO_3)(OH)^{3-}$ inhibited the U(VI) adsorption, which decreased the adsorption capacity[57]. Therefore, an optimal pH of 3.0 was used in subsequent experiments. In addition, the ion strength clearly had little effect on the adsorption process, which suggests that the inner-sphere surface complexation mechanism plays a main role in the adsorption process[58].

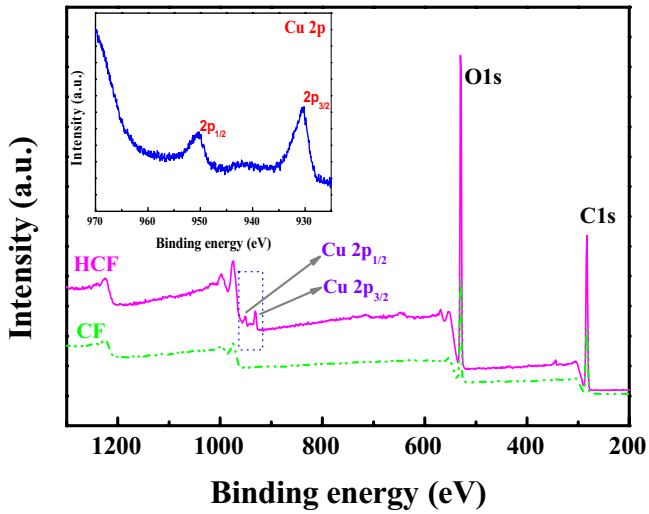

Figure 2. XPS survey spectra of HCF and CF. Insert: high-resolution Cu 2p spectra of HCF.

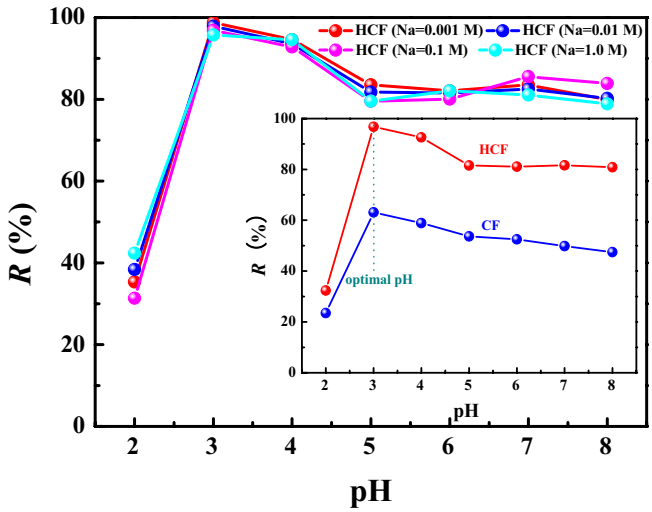

Figure 3. Effect of the ion strength on the removal rate. Insert: effect of pH on the removal rate (pH = 3.0, m/V = 0. 5 g L^{-1}, C_0 = 10 mg L^{-1} and contact time = 30 min).

Effect of the contact time and kinetic studies. The adsorption efficiency of the adsorbents can be evaluated by the adsorption equilibrium time and kinetic process. Figure 4 presents the effect of the contact time of 5–120 min on the U(VI) sorption by HCF and CF in regard to the kinetics at an initial U(VI) concentration of 10 mg L^{-1} at pH 3.0 at room temperature. With the extension of time, the adsorption efficiency significantly increased until it reached an equilibrium within 30 min. The removal rate of HCF for U(VI) was nearly 100% within 30 min, while the removal efficiency of CF was poor (only approximately 70%). Pseudo-first-order and pseudo-second-order models were used to study the adsorption kinetics of U(VI) on HCF. Figure 4 (insert) clearly shows that the pseudo-second-order model had a superior correlation coefficient (R^2) compared to the pseudo-first-order model, which indicates that the U(VI) adsorption processes of HCF well fit the pseudo-second-order model.

Adsorption isotherms and thermodynamic studies. Langmuir and Freundlich adsorption isotherm models are expressed in Eqs. (1) and (2), respectively[59]. According to Eqs. (1) and (2), the maximal adsorption capacity (Q_m) was fitted when the initial U(VI) concentration was 5–150 mg L^{-1} (Fig. 5). The calculated Langmuir and Freundlich isotherm parameters from the fitting processes are listed in Table 1. Table 1 shows that Langmuir isotherm fitted the experimental data well with a higher correlation coefficient (R^2), and the maximum adsorption capacity was 241.28 mg g^{-1} for the adsorption of HCF. Moreover, Fig. 5 shows that HCF is a promising sorbent for the removal of uranium from aqueous solutions in terms of the preparation cost, adsorption efficiency and simple solid–liquid separation for uranium from aqueous solutions.

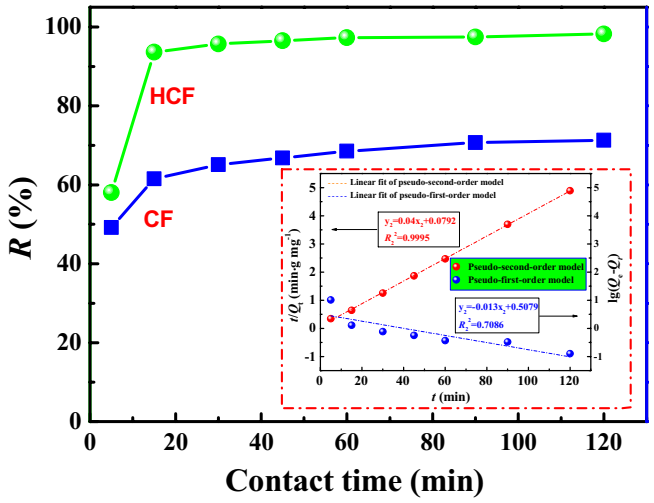

Figure 4. Effect of the contact time on the U(VI) sorption (pH = 3.0, $C_{(U)initial}$ = 10 mg L^{-1} and m/V = 0.4 g L^{-1}). Insert: linear fit of the pseudo-first-order and pseudo-second-order kinetics models.

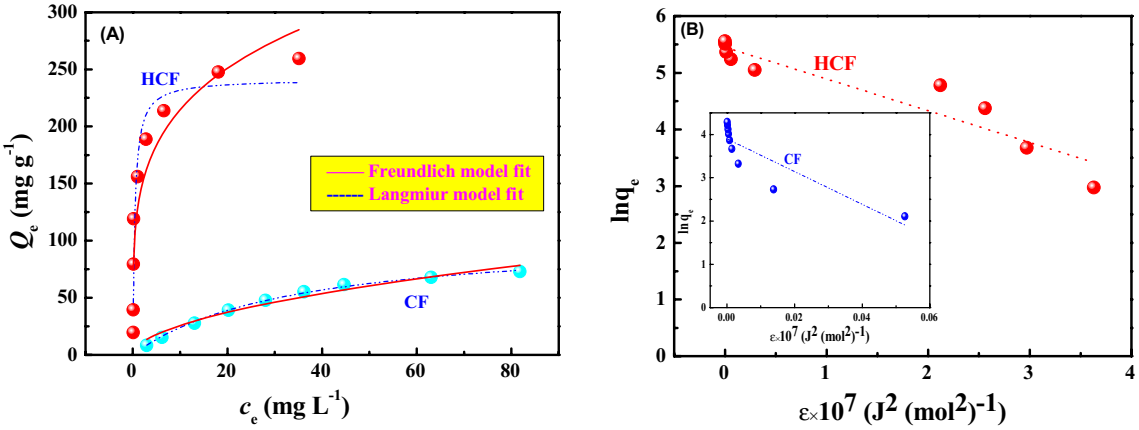

Figure 5. Langmuir, Freundlich model fit (**A**) and D–R isotherm plots (**B**) of U(VI) onto HCF and CF (pH = 3.0, $C_{(U)initial}$ = 5–150 mg L^{-1}, m/V = 0.4 g L^{-1} and contact time = 24 h).

Sorbents	Langmuir			Freundlich			D-R			
	Q_m mg g^{-1}	k_L L mg^{-1}	R^2	n	k_F mg^{1-n} L^n g^{-1}	R^2	q_s mg g^{-1}	β mol^2 $(J^2)^{-1}$	E kJ mol^{-1}	R^2
HCF	241.28	2.418	0.9152	4.45	127.91	0.8466	232.93	0.56	0.56	0.8724
CF	104.56	0.029	0.9976	1.89	7.6110	0.9629	49.34	37.81	0.12	0.7363

Table 1. Langmuir, Freundlich and D–R isotherm model parameters for U(VI) adsorption onto HCF and CF.

$$Q_e = \frac{Q_m \cdot K_L \cdot C_e}{1 + K_L C_e}, \tag{1}$$

$$Q_e = K_F \cdot C_e^{1/n}, \tag{2}$$

where Q_e (mg g^{-1}) is the equilibrium adsorption capacity; C_e (mg L^{-1}) is the uranium concentration at equilibrium; Q_m (mg g^{-1}) is the maximum adsorption capacity; K_L (L mg^{-1}) and K_F (mg^{1-n} L^n g^{-1}) are Langmuir constant and Freundlich constant, respectively; n is Freundlich adsorption exponent.

Dubinin–Radushkevich (D–R) isotherm is usually employed to explain the adsorption mechanism with respect to Gaussian energy distribution onto a heterogeneous surface and determine the adsorption nature as physical or chemical based on the mean free energy (E)[60]. The D–R isotherm model is expressed by Eq. (3). Model parameters ε, β and E can be determined and calculated by Eqs. (4) and (5).

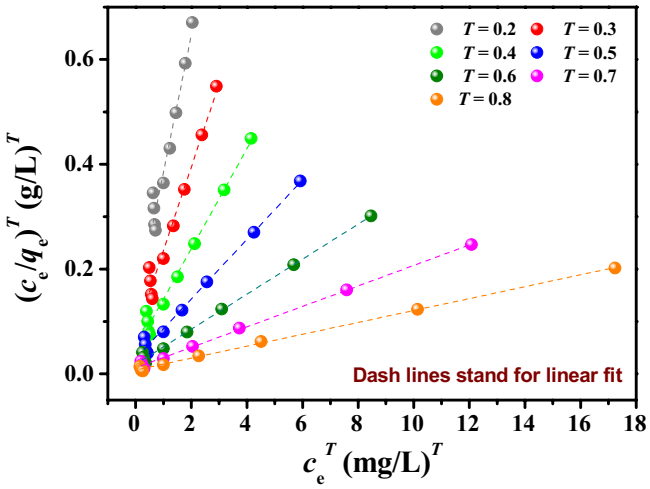

Figure 6. Linear fit of the Toth equation at different T for the adsorption of uranium on HCF.

	Parameters of the Toth equations		
T	q_T (mg/g)	b_T (L/mg)	R^2
0.2	841.65	40.53	0.9548
0.3	468.97	11.47	0.9718
0.4	359.49	5.81	0.9832
0.5	318.88	3.73	0.9903
0.6	288.69	2.70	0.9944
0.7	277.21	2.10	0.9966
0.8	269.64	1.71	0.9977

Table 2. Parameters of the Toth equations in the adsorption of uranium on HCF.

$$\ln Q_e = \ln Q_m - \beta\varepsilon^2, \tag{3}$$

$$\varepsilon = RT \ln (1 + 1/C_e), \tag{4}$$

$$E = \frac{1}{\sqrt{2\beta}}, \tag{5}$$

where β (mol^2 (J^2)$^{-1}$) is D–R isotherm constant, and ε (J mol^{-1}) is Polanyi potential. The calculated D–R isotherm parameters are listed in Table 1. From the obtained E value, the physical or chemical sorption mechanism can be revealed. According to the literature[61], if E is 8–16 kJ mol^{-1}, the sorption process chemically occurs, whereas $E < 8$ kJ mol^{-1} follows the physical sorption. For HCF, the low E value of 0.56 kJ mol^{-1} in this study suggests that the U adsorption was a physical adsorption process due to electrostatic or Van der Waal's attractions.

The linear form of the Toth equation was as following[62]. A linear relationship can be obtained by plotting $(c_e/q_e)^T$ against $(c_e)^T$ at different T values, and then the values of q_T, b_T and R^2 can be calculated.

$$\left(\frac{c_e}{q_e}\right)^T = \frac{1}{(q_T b_T)^T} + \frac{1}{q_T^T} c_e^T, \tag{6}$$

where q_T (mg g^{-1}) and b_T (L mg^{-1}) are the parameters of the Toth equation, T is exponent of the Toth equation.

Figure 6 shows the regression results for the adsorption of uranium on HCF. The best regression line is identified when T is above 0.8 and the R^2 value of the line is closest to 1. The calculated values of q_T, b_T and R^2 are also listed in Table 2. Table 2 indicates that the values of R^2 increase with the increase of the values of T. As a result, the Toth equation ($T > 0.8$) reveals better-fitting results than the Langmuir, Freundlich and D–R equations. According to the reference[63], T is 0.6–1.0 for the adsorption of uranium, meaning that the adsorption occurs mostly on homogeneous surfaces in this study.

A comparison of the maximum adsorption capacity (Q_m) of various adsorbents is shown in Table 3. According to Table 3, the as-synthesized HCF clearly presents higher Q_m than other cellulose-based adsorbents. This increased adsorption capacity of HCF for U(VI) may be attributed to its fibrous structure and the addition of HST

Cellulose-based sorbents	pH	m/V (g L^{-1})	Q_m (mg g^{-1})	References
Amine-impregnated cellulose	0.1–3.0	2.5	54.5	[43]
Urea-cellulose	0.1–3.0	2.5	82	[44]
CMC-Al	5.0	–	12.1	[45]
HPMC-g-AO film	4.1	–	765	[48]
Polyacrylonitrile fibres	5.0	1.0	163	[6]
Graphene oxide-cellulose	5.0	1.0	101.01	[66]
CMC/MGOs	5.5	0.25	188.97	[67]
CSP-CMCP	5.0	0.05	977.54	[68]
Arg-Cell, Glu-Cell	5.0	0.4	147, 168	[69]
SA/CMC-Ca-Al	4.0	–	101.76	[70]
CMC-FeS	5.0	–	430.3	[71]
P(IA/MAA)-g-NC/NB	5.5	2.0	119.63	[72]
CMC-INP	5.0	–	322.58	[73]
HCF	3.0	0.4	241.28	This study

Table 3. Maximum adsorption capacity (Q_m) of cellulose-based adsorbents for U(VI) ions.

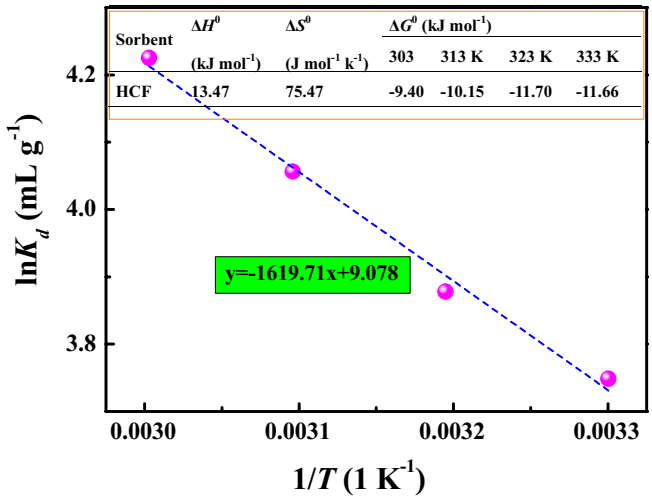

Figure 7. $\ln K_d$ versus $1/T$ for U(VI) adsorption onto HCF. pH = 3.0, $C_{(U)initial}$ = 10 mg L^{-1}, $C_{sorbent}$ = 0.4 g L^{-1}, T = 303 K, 313 K, 323 K and 333 K, and contact time = 24 h.

with higher specific surface area and excellent adsorption efficiency[64] in the surface of CF. Q_m of the as-prepared HCF shows that HCF is a promising adsorbent for the treatment of uranium-bearing wastewater.

To evaluate the adsorption thermodynamic parameters, the effect of temperature on the uranium removal was investigated using 20 mL solutions containing 0.008 g of HCF and 10 mg L^{-1} U(VI), which was shaken for 24 h at pH 3.0. After the adsorption equilibrium, adsorption results of U(VI) by HCF were obtained, and the plots of $\ln K_d$ versus $1/T$ onto HCF is shown in Fig. 7. Thermodynamic parameters (i.e., enthalpy (ΔH^0), entropy (ΔS^0) and standard free energy ΔG^0) from 303 to 333 K in the adsorption process were calculated from the slope and intercept of the linear line of $\ln K_d$ versus $1/T$ according to Vander Hoff Eqs. (7) ~ (9)[65]. The evaluated ΔH^0 value is 13.47 kJ mol^{-1}, which reflects that the adsorption reaction was endothermic. The obtained positive ΔS^0 and negative ΔG^0 values (Fig. 7 insert) suggest that the adsorption process was spontaneous.

$$K_d = \frac{c_{ad}}{c_e}, \tag{7}$$

$$\ln K_d = -\frac{\Delta H^0}{RT} + \frac{\Delta S^0}{R}, \tag{8}$$

$$\Delta G^0 = \Delta H^0 - T\Delta S^0, \tag{9}$$

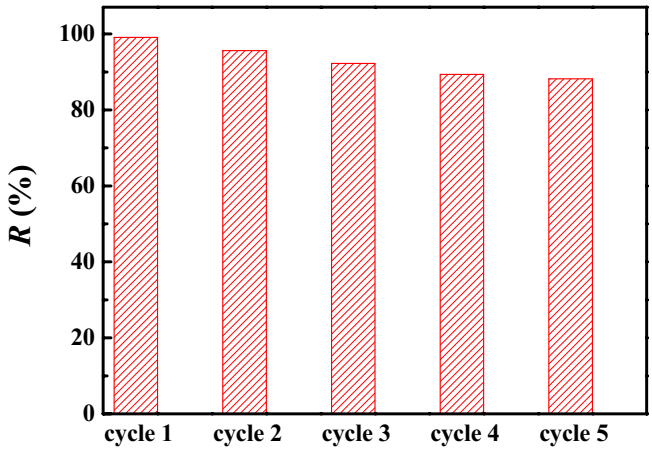

Figure 8. Regeneration and reuse studies of HCF (pH = 3.0, $C_{(U)initial}$ = 10 mg L^{-1}, m/V = 0.40 g L^{-1} and contact time = 24 h).

where K_d (mL g^{-1}) is the distribution coefficient of U(VI); c_{ad} (mg L^{-1}) is the concentration of metal ions on the adsorbent at equilibrium; c_e (mg L^{-1}) is the equilibrium concentration of metal ions in solution; R (8.314 J mol^{-1} K^{-1}) is the universal gas constant; T (K) is the absolute temperature.

Regeneration and reuse of HCF. The adsorbent reuse is an important index to further evaluate their adsorption performance and reduce the treatment cost. After adsorption and filtration, the adsorbent loaded U(VI) was collected and treated with excess HNO_3 (0.1 mol L^{-1}) for 24 h in a shaker. Then, the adsorbent was separated from the liquid by filtration and washed several times by DW to be used for the next cycle adsorption experiment. The reuse experiments of HCF were performed for five cycles. According to Fig. 8, the U(VI) removal percentage with HCF was 99.11% after the first cycling experiment. After five recycling experiments, the U(VI) removal percentage remained at 88.24%, which suggests that HCF can be recovered and reused several times and has favourable recycling capability.

Materials and methods

Materials. The cotton fibre (CF) in this study was medical purified cotton from Xvzhou hygienic materials plant (Jiangsu, China). Copper(II) nitrate trihydrate ($Cu(NO_3)_2{\cdot}3H_2O$) was provided by Chengdu Kelong Chemical Co., Ltd. Benzoic acid (BA), and trimesic acid (H_3BTC) was purchased from Aladdin Chemical Reagent Co., Ltd. All reagents were of analytical grade and used without further purification. $UO_2(NO_3)_2{\cdot}6H_2O$ was provided by Xi'an Dingtian Chemical Reagent Co., Ltd. The deionized water (DW) was used throughout the experiments.

Synthesis. HCF was synthesized through a simple solvothermal method. In a typical synthesis of HCF, 1.0870 g of $Cu(NO_3)_2{\cdot}3H_2O$ was dissolved in 15 mL DW. The mixture of 0.3948 of H_3BTC and 0.0769 g of BA was dissolved in 15 mL absolute ethanol. Then, both solutions were mixed and stirred for 30 min. The resulting mixture and 0.5 g of CF were transferred into a Teflon autoclave and heated in an oven at 110 ℃ for 24 h. The resultant blue fibrous products (HCF) were filtered in vacuum and completely washed by ethanol and DW. Finally, the products were dried at 100 ℃ in vacuum.

In the above preparation process of HCF, by the hydrothermal synthesis method firstly H_3BTC react with BA in a Teflon autoclave to obtain the MOF product (noted as HST), and then HST composites with the raw material CF to produce HCF.

Characterization. The structure characteristics of HCF, CF and HST were analysed by Fourier transform infrared (FTIR) spectroscopy (Bruker VERTEX 70, Germany). The morphology characteristics of the samples were obtained on a scanning electron microscope (SEM) (Helios 600i, Japan). X-ray photoelectron spectroscopy (XPS) of HCF and CF were studied using an ESCALAB 250 X-ray photoelectron spectroscope (Thermo fisher, USA). Thermal stability of the products was studied by thermogravimetric analysis (TGA) spectroscopy (Netzsch STA449F5, Germany) from 30 to 900 ℃ at a heating rate of 10 K/min under an argon flow.

Adsorption studies. The U(VI) stock solutions were prepared by dissolving $UO_2(NO_3)_2{\cdot}6H_2O$ in DW; then, small amounts of concentrated HNO_3 was added to avoid the hydrolysis of UO_2^{2+}. The working U(VI) solutions were prepared by appropriately diluting the stock solutions immediately before their use. The adsorption capacities of U(VI) onto HCF and CF were investigated as a function of the solution pH, contact time, initial U concentration and temperature by batch adsorption experiments. The solution pH was adjusted by adding NaOH and HCl and measured using a glass electrode (Leici PHS-3C, China). HCF or CF was added to 20 mL U(VI) solution and shaken in a shaker (Kangshi, China). After filtration, the U(VI) concentration in the solution was determined by a micro-quantity uranium analyser (MUA model, China). All experiments were performed in

triplicate, and the data are presented as the mean values. The removal efficiency (R (%)) and adsorption amount of U(VI) on HCF or CF (q (mg g^{-1})) of U(VI) in solution were calculated using Eqs. (10) and (11)[59], respectively.

$$R(\%) = \frac{c_0 - c_t}{c_0} \times 100, \tag{10}$$

$$q(mg \cdot g^{-1}) = \frac{(c_0 - c_t)}{m} \times V, \tag{11}$$

where c_0 (mg L^{-1}) is the initial U(VI) concentration, c_t (mg L^{-1}) is the U(VI) concentration at time t in the solution, V (L) is the solution volume, and m (g) is the adsorbent mass.

In the desorption experiments, the obtained U(VI)-loaded HCF was washed with DW and rinsed in 3 M HNO_3 for 24 h; then, it was thoroughly washed in DW until U(VI) ions were not detected in the rinsing solution. The dried and regenerated adsorbent was reused for further adsorption experiments, and this recycling procedure was repeated five times.

Conclusion

The composite HCF with lower cost was fabricated via a facile solvothermal approach to adsorb U(VI) from aqueous solutions. The preparation cost of the adsorbent was significantly reduced by using BA with lower cost as the ligand to replace part of the traditional ligand H_3BTC. HCF shows favourable adsorption capacity for U(VI) with maximum adsorption capacities of 241.28 mg g^{-1} at pH 3.0 compared to CF. HCF shows favourable regenerability, and the U(VI) removal percentage was 88.24% after five cycles. This work offers a new and cost-effective adsorbent HCF, which can be effectively used as a promising sorbent to remove U(VI) from the real multi-component U(VI)-containing nuclear waste influents. Furthermore, due to the advantageous fibrous form, HCF can be easily separated from aqueous solutions, which enhances post-treatment efficiency for further practical applications.

Received: 20 June 2020; Accepted: 19 October 2020
Published online: 06 November 2020

References

1. Xiong, Y. Y. *et al.* MOF catalysis of Fe^{II}-to-Fe^{III} reaction for an ultrafast and one-step generation of the Fe_2O_3@MOF composite and uranium(VI) reduction by iron(II) under ambient conditions. *Chem. Commun.* **52**, 9538–9541 (2016).
2. Luo, W. *et al.* Engineering robust metal-phenolic network membranes for uranium extraction from seawater. *Energy Environ. Sci.* **12**, 607–614 (2019).
3. Liu, W. J. *et al.* Efficiency and mechanism of adsorption of low-concentration uranium from water by a new chitosan/aluminum sludge composite aerogel. *Dalton Trans.* **49**(10), 3209–3221 (2020).
4. Abney, C. W., Mayes, R. T., Saito, T. & Dai, S. Materials for the recovery of uranium from seawater. *Chem. Rev.* **117**, 13935–14013 (2017).
5. Sun, Q. *et al.* Bio-inspired nano-traps for uranium extraction from seawater and recovery from nuclear waste. *Nat. Commun.* **9**, 1644 (2018).
6. Wang, F. *et al.* Study of adsorption performance and adsorption mechanism for U(VI) ion on modified polyacrylonitrile fibers. *J. Radioanal. Nucl. Chem.* **323**, 365–377 (2020).
7. Huang, S. Y. *et al.* Dual functional nanocomposites of magnetic $MnFe_2O_4$ and fluorescent carbon dots for efficient U(VI) removal. *Chem. Eng. J.* **368**, 941–950 (2019).
8. Xie, Y. *et al.* Emerging natural and tailored materials for uranium-contaminated water treatment and environmental remediation. *Prog. Mater. Sci.* **103**, 180–234 (2019).
9. Garza-Cervantes, J. A. *et al.* Antimicrobial activity of a silver-microfibrillated cellulose biocomposite against susceptible and resistant bacteria. *Sci. Rep.* **10**, 7281 (2020).
10. Hausmann, M. K. *et al.* Complex-shaped cellulose composites made by wet densification of 3D printed scaffolds. *Adv. Funct. Mater.* **30**, 1904127 (2020).
11. Guo, L. F., Li, D. F., Lennholm, H., Zhai, H. M. & Ek, M. Structural and functional modification of cellulose nanofibrils using graft copolymerization with glycidyl methacrylate by Fe^{2+}–thiourea dioxide–H_2O_2 redox system. *Cellulose* **26**, 4853–4864 (2019).
12. Liu, X. L. *et al.* Improving salt tolerance and thermal stability of cellulose nanofibrils by grafting modification. *Carbohyd. Polym.* **211**, 257–265 (2019).
13. Li, M. F. *et al.* PVA-co-PE nanofiber/epoxy composites with cellulose nanocrystals. *Compos. Sci. Technol.* **188**, 107990 (2020).
14. Chen, W., Yuan, Y. & Chen, Y. L. Visualized bond scission in mechanochemiluminescent polymethyl acrylate/cellulose nanocrystals composites. *ACS Macro Lett.* **9**(4), 438–442 (2020).
15. Onur, A., Ng, A., Garnier, G. & Batchelor, W. The use of cellulose nanofibres to reduce the wet strength polymer quantity for development of cleaner filters. *J. Clean. Prod.* **215**, 226–231 (2019).
16. Chen, J. *et al.* Direct reduction of graphene oxide/nanofibrillated cellulose composite film and its electrical conductivity research. *Sci. Rep.* **10**, 3124 (2020).
17. Cui, W. G., Hu, T. L. & Bu, X. H. Metal-organic framework materials for the separation and purification of light hydrocarbons. *Adv. Mater.* **32**, 1806445 (2020).
18. Lo, S. H. *et al.* Rapid desolvation-triggered domino lattice rearrangement in a metal-organic framework. *Nat. Chem.* **90**, 90–97 (2020).
19. Knebel, A. *et al.* Defibrillation of soft porous metal-organic frameworks with electric fields. *Science* **358**, 347–351 (2017).
20. Wu, S. Y., Min, H., Shi, W. & Cheng, P. Multicenter metal-organic framework-based ratiometric fluorescent sensors. *Adv. Mater.* **32**, 18058 (2020).
21. Zheng, J. *et al.* Molecular insight into fluorocarbon adsorption in pore expanded metal–organic framework analogs. *J. Am. Chem. Soc.* **142**, 3002–3012 (2020).
22. Bhadra, B. N., Yoo, D. K. & Jhung, S. H. Carbon-derived from metal–organic framework MOF-74: A remarkable adsorbent to remove a wide range of contaminants of emerging concern from water. *Appl. Surf. Sci.* **504**, 144348 (2020).
23. Dhaka, S. *et al.* Metal–organic frameworks (MOFs) for the removal of emerging contaminants from aquatic environments. *Coord. Chem. Rev.* **380**, 330–352 (2019).

24. Pang, Y. C. *et al.* Metal–organic framework nanoparticles for ameliorating breast cancer-associated osteolysis. *Nano Lett.* **20**, 829–840 (2020).
25. Gonzalez, M. I. *et al.* Confinement of atomically defined metal halide sheets in a metal–organic framework. *Nature* **577**, 64–68 (2020).
26. Wang, Z. *et al.* Breathing-ignited long persistent luminescence in a resilient metal–organic Framework. *Chem. Mater.* **32**, 841–848 (2020).
27. Yu, F. *et al.* Enhancing the separation efficiency of a C_2H_2/C_2H_4 mixture by a chromium metal–organic framework fabricated via post-synthetic metalation. *J. Mater. Chem. A* **8**, 2083–2089 (2020).
28. Xin, Z. F. *et al.* Metallocene implanted metalloporphyrin organic framework for highly selective CO_2 electroreduction. *Nano Energy* **67**, 104233 (2020).
29. Yang, W. P. *et al.* Applications of metal–organic-framework-derived carbon materials. *Adv. Mater.* **31**, 1804740 (2019).
30. Jiang, Z. W. *et al.* Controllable synthesis of porphyrin-based 2D lanthanide metal–organic frameworks with thickness- and metal-node-dependent photocatalytic performance. *Angew. Chem.-Int. Edit.* **59**, 3300–3306 (2020).
31. Wang, Z. X. *et al.* Metal–organic frameworks and their derivatives with graphene composites: Preparation and applications in electrocatalysis and photocatalysis. *J. Mater. Chem. A* **8**, 2934–2961 (2020).
32. Zhou, S. Y., Strømme, M. & Xu, C. Highly transparent, flexible, and mechanically strong nanopapers of cellulose nanofibers@ metal–organic Frameworks. *Chem. Eur. J.* **3**, 3515–3520 (2019).
33. Ma, S. S. *et al.* Multifunctional cellulose-based air filters with high loadings of metal–organic frameworks prepared by in situ growth method for gas adsorption and antibacterial applications. *Cellulose* **25**, 5999–6010 (2018).
34. Rickhoff, T. A., Werth, L. K., Kissel, D. S., Keleher, J. J. & Sullivan, E. A biomimetic cellulose-based composite material that incorporates the antimicrobial metal-organic framework HKUST-1. *J. Appl. Polym. Sci.* https://doi.org/10.1002/APP.46978 (2019).
35. Wang, C., Qian, X. R. & An, X. H. In situ green preparation and antibacterial activity of copper-based metal–organic frameworks/cellulose fibers (HKUST-1/CF) composite. *Cellulose* **22**, 3789–3797 (2015).
36. Rodríguez, H. S. *et al.* Antibacterial activity against escherichia coli of Cu-BTC (MOF-199) metal-organic framework immobilized onto cellulosic fibers. *J. Appl. Polym. Sci.* https://doi.org/10.1002/APP.40815 (2014).
37. Duan, C. *et al.* Synthesis of novel cellulose- based antibacterial composites of Ag nanoparticles@ metal–organic frameworks@ carboxymethylated fibers. *Carbohyd. Polym.* **193**, 82–88 (2018).
38. Yang, Q., Zhang, M. Y., Song, S. X. & Yang, B. Surface modification of PCC filled cellulose paper by MOF-5 ($Zn_3(BDC)_2$) metal–organic frameworks for use as soft gas adsorption composite materials. *Cellulose* **24**, 3051–3060 (2017).
39. Lu, H. L. *et al.* Cellulose-supported magnetic Fe_3O_4–MOF composites for enhanced dye removal application. *Cellulose* **26**, 4909–4920 (2019).
40. Cui, X. F. *et al.* In-situ fabrication of cellulose foam HKUST-1 and surface modification with polysaccharides for enhanced selective adsorption of toluene and acidic dipeptides. *Chem. Eng. J.* **369**, 898–907 (2019).
41. Shen, C. K. *et al.* Catalytic MOF-loaded cellulose sponge for rapid degradation of chemical warfare agents simulant. *Carbohyd. Polym.* **213**, 184–191 (2019).
42. Lange, L. E. & Obendorf, S. K. Functionalization of cotton fiber by partial etherification and self-assembly of polyoxometalate encapsulated in $Cu_3(BTC)_2$ metal–organic framework. *ACS Appl. Mater. Inter.* **7**, 3974–3980 (2015).
43. Orabi, A. H. *et al.* Potentiality of uranium adsorption from wet phosphoric acid using amine-impregnated cellulose. *J. Radiat. Res. Appl. Sci.* **9**, 193–206 (2016).
44. Orabi, A. H. Synthesis of a cellulose derivative for enhanced sorption and selectivity of uranium from phosphate rocks prior to its fluorometric determination. *Int. J. Environ. Anal. Chem.* **99**(8), 741–766 (2019).
45. Wu, L. P., Lin, X. Y., Du, X. C. & Luo, X. G. Biosorption of uranium(VI) from aqueous solution using microsphere adsorbents of carboxymethyl cellulose loaded with aluminum(III). *J. Radioanal. Nucl. Chem.* **310**, 611–622 (2016).
46. Rule, P., Balasubramanian, K. & Gonte, R. R. Uranium(VI) remediation from aqueous environment using impregnated cellulose beads. *J. Environ. Radioactiv.* **136**, 22–29 (2014).
47. Yousif, A. M., El-Afandy, A. H., Wahab, G. M. A., Mubark, A. E. & Ibrahim, I. A. Selective separation of uranium(VI) from aqueous solutions using amine functionalized cellulose. *J. Radioanal. Nucl. Chem.* **303**, 1821–1833 (2015).
48. Başarır, S. Ş & Bayramgil, N. P. The uranium recovery from aqueous solutions using amidoxime modified cellulose derivatives. IV. Recovery of uranium by amidoximated hydroxypropyl methylcellulose. *Cellulose* **20**, 827–839 (2013).
49. Anirudhan, T. S. & Sreekumari, S. S. Synthesis and characterization of a functionalized graft copolymer of densified cellulose for the extraction of uranium(VI) from aqueous solutions. *Colloid. Surface. A* **361**, 180–186 (2010).
50. Anirudhan, T. S., Nima, J. & Divya, P. L. Adsorption and separation behavior of uranium(VI) by 4-vinylpyridine-grafted-vinyltriethoxysilane-cellulose ion imprinted polymer. *J. Environ. Chem. Eng.* **3**, 1267–1276 (2015).
51. Villalobos-Rodríguez, R., Montero-Cabrera, M. E., Esparza-Ponce, H. E., Herrera-Peraza, E. F. & Ballinas-Casarrubias, M. L. Uranium removal from water using cellulose triacetate membranes added with activated carbon. *Appl. Radiat. Isotopes* **70**, 872–881 (2012).
52. Zolfonoun, E. & Yousefi, S. R. On-line extraction and determination of uranium in aqueous samples using multi-walled carbon nanotubes-coated cellulose acetate membrane. *Int. J. Environ. Anal. Chem.* **96**(3), 203–211 (2016).
53. Lin, K. Y. A. & Hsieh, Y. T. Copper-based metal organic framework (MOF), HKUST-1, as an efficient adsorbent to remove p-nitrophenol from water. *J. Taiwan Inst. Chem. E.* **50**, 223–228 (2015).
54. Gu, C. M. *et al.* Ultrasensitive non-enzymatic pesticide electrochemical sensor based on HKUST-1-derived copper oxide @ mesoporous carbon composite. *Sens. Actuators B Chem.* **305**, 127478 (2020).
55. Wang, W. X., Chen, Z., Zhou, H. J., Zhang, Y. F. & Wang, X. K. Two-dimensional lamellar magnesium silicate with large spacing as an excellent adsorbent for uranium immobilization. *Environ. Sci. Nano* **5**, 2406–2414 (2018).
56. Li, M. X., Liu, H. B., Chen, T. H., Dong, C. & Sun, Y. B. Synthesis of magnetic biochar composites for enhanced uranium (VI) adsorption. *Sci. Total Environ.* **651**, 1020–1028 (2019).
57. Meng, J. *et al.* Adsorption capacity of kelp-like electrospun nanofibers immobilized with bayberry tannin for uranium(VI) extraction from seawater. *RSC Adv.* **9**, 8091–8103 (2019).
58. Zhu, J. H. *et al.* Metal–organic frameworks (MIL-68) decorated graphene oxide for highly efficient enrichment of uranium. *J. Taiwan Inst. Chem. E.* **99**, 45–52 (2019).
59. Yu, S. J. *et al.* Efficient removal of uranium(VI) by layered double hydroxides supported nanoscale zero-valent iron: A combined experimental and spectroscopic studies. *Chem. Eng. J.* **365**, 51–59 (2019).
60. Muthukumaran, C., Sivakumar, V. M. & Thirumarimurugan, M. Adsorption isotherms and kinetic studies of crystal violet dye removal from aqueous solution using surfactant modified magnetic nanoadsorbent. *J. Taiwan Inst. Chem. E.* **63**, 354–362 (2016).
61. Liu, R., Zhang, W., Chen, Y. T. & Wang, Y. S. Uranium (VI) adsorption by copper and copper/iron bimetallic central MOFs. *Colloid. Surface. A.* https://doi.org/10.1016/j.colsurfa.2019.124334 (2020).
62. Wu, K. T., Wu, P. H., Wu, F. C., Jreng, R. L. & Juang, R. S. A novel approach to characterizing liquid-phase adsorption on highly porous activated carbons using the Toth equation. *Chem. Eng. J.* **221**, 373–381 (2013).
63. Toth, J. Uniform interpretation of gas/solid adsorption. *Adv. Colloid Interface Sci.* **55**, 1–239 (1995).
64. Yang, A. L., Li, P. & Zhong, J. R. Facile preparation of low-cost HKUST-1 with lattice vacancies and high-efficiency adsorption for uranium. *RSC Adv.* **9**, 10320–10325 (2019).

65. Abdi, S., Nasiri, M., Mesbahi, A. & Khani, M. H. Investigation of uranium (VI) adsorption by polypyrrole. *J. Hazard. Mater.* **332**(1), 132–139 (2017).
66. Yang, A. L., Wu, J. H. & Huang, C. P. Graphene oxide-cellulose composite for the adsorption of uranium(VI) from dilute aqueous solutions. *J. Hazard. Toxic Radioact. Waste* **22**(2), 04017029 (2018).
67. Zong, P. F. *et al.* Carboxymethyl cellulose supported magnetic graphene oxide composites by plasma induced technique and their highly efficient removal of uranium ions. *Cellulose* **26**, 4039–4060 (2019).
68. Cai, Y. W. *et al.* Rational synthesis of novel phosphorylated chitosan-carboxymethyl cellulose composite for highly effective decontamination of U(VI). *ACS Sustain. Chem. Eng.* **7**, 5393–5403 (2019).
69. El-Bohy, M. N. *et al.* Grafting of arginine and glutamic acid onto cellulose for enhanced uranyl sorption. *Cellulose* **24**, 1427–1443 (2017).
70. Wu, L. P., Lin, X. Y., Zhou, X. B. & Luo, X. G. Removal of uranium and fluorine from wastewater by double-functional microsphere adsorbent of SA/CMC loaded with calcium and aluminum. *Appl. Surf. Sci.* **384**, 466–479 (2016).
71. Shao, D. D. *et al.* Immobilization of uranium by biomaterial stabilized FeS nanoparticles: Effects of stabilizer and enrichment mechanism. *J. Hazard. Mater.* **302**, 1–9 (2016).
72. Anirudhan, T. S., Deepa, J. R. & Binusreejayan. Synthesis and characterization of multi-carboxyl-functionalized nanocellulose/nanobentonite composite for the adsorption of uranium(VI) from aqueous solutions: Kinetic and equilibrium profiles. *Chem. Eng. J.* **273**, 390–400 (2015)
73. Popescu, I. C. *et al.* Removal of uranium (VI) from aqueous systems by nanoscale zero-valent iron particles suspended in carboxymethyl cellulose. *J. Nucl. Mater.* **443**, 250–255 (2013).

Acknowledgements

This work is financially supported by National Natural Science Foundation of China (21407132) and Environmental Protection Foundation of China Academy of Engineering Physics (No. YAHZY-2018-008).

Author contributions

A.Y. contributed to the experiments design and carried out the adsorbents preparation and adsorption experiments. Z.W. and Y.Z. performed the adsorption tests. A.Y. prepared the figures and wrote the manuscript.

Competing interests

The authors declare no competing interests.

Additional information

Correspondence and requests for materials should be addressed to A.Y.

Reprints and permissions information is available at www.nature.com/reprints.

Publisher's note Springer Nature remains neutral with regard to jurisdictional claims in published maps and institutional affiliations.

Open Access This article is licensed under a Creative Commons Attribution 4.0 International License, which permits use, sharing, adaptation, distribution and reproduction in any medium or format, as long as you give appropriate credit to the original author(s) and the source, provide a link to the Creative Commons licence, and indicate if changes were made. The images or other third party material in this article are included in the article's Creative Commons licence, unless indicated otherwise in a credit line to the material. If material is not included in the article's Creative Commons licence and your intended use is not permitted by statutory regulation or exceeds the permitted use, you will need to obtain permission directly from the copyright holder. To view a copy of this licence, visit http://creativecommons.org/licenses/by/4.0/.

© The Author(s) 2020